

Hydrodynamic coupling in polygonal arrays of colloids: Experimental and analytical resultsGiovanni M. Cicuta,¹ Jurij Kotar,² Aidan T. Brown,² Ji-Ho Noh,² and Pietro Cicuta²¹*Dip. Fisica, Università di Parma and INFN, Sez. Milano-Bicocca, Gruppo di Parma, Italy*²*Cavendish Laboratory and Nanoscience Centre, University of Cambridge, Cambridge CB3 0HE, United Kingdom*

(Received 13 April 2010; published 18 May 2010)

Colloidal particles are trapped harmonically on the vertices of planar regular polygons, using optical tweezers. The particles interact with each other via hydrodynamic coupling, which can be described adequately by Oseen's tensor. Because of the interaction, the dynamics of any individual sphere is complex. Thermal motion results in a spectrum of relaxation times. The configuration of a system of N particles can be decomposed into $2N$ normal modes. In this work it is shown how to calculate these modes and their relaxation time scale analytically. The mathematical structure of the matrix of interaction leads to general properties for the symmetry of the normal modes and their dynamics, differing between the cases of even and odd N . The theory is compared to experiments performed on a range of rings with $3 \leq N \leq 10$, varying also the trap stiffness and the distance between particles.

DOI: [10.1103/PhysRevE.81.051403](https://doi.org/10.1103/PhysRevE.81.051403)

PACS number(s): 82.70.Dd, 87.80.Cc, 05.60.Cd

I. INTRODUCTION

Colloidal particles are subject to a variety of direct interactions, which can be tuned and controlled to make excellent model systems or industrial products. Colloidal particles are also coupled to each other hydrodynamically. This is a qualitatively different interaction, depending on the interparticle velocity as well as the spatial configuration. In contrast to direct interactions which can be effectively switched off, hydrodynamic coupling can be tuned but never completely screened. The motion of one particle always causes flow which influences other neighboring particles. Hydrodynamic coupling is an important feature in biological flows [1] and is thought, for example, to be at the root of synchronization of cilia beats, leading to metachronal waves [2,3]. It appears in natural and artificial microfluidic conditions [4,5] and can be put to use in swimming or pumping strategies at low Reynolds number (Re) [6–9]. For the case of spherical particles, Oseen calculated the form of interaction in the far-field limit that is when the distance between the spheres is much larger than their diameter [10]. As a further consequence of hydrodynamic interaction, there are correlations in the Brownian fluctuations of different particles. This is well known, and indeed exploited, in two-particle passive microrheology, where the statistical correlation in the motion of two tracer particles enables one to extract the solvent viscosity (and even the viscoelasticity in complex fluids) [11,12]. To maintain an average distance and acquire good statistics, the tracer spheres can be trapped by focused laser beams, effectively confining each bead in a harmonic well. In this scenario the average position of the spheres is well defined, but the beads are constantly subjected to thermal fluctuations which displace them from the minimum of the trap potential. In liquids, optically trapping spheres of colloidal sizes, the relaxation dynamics is always overdamped; an investigation of underdamped hydrodynamic interaction was carried out on water droplets suspended in air [13]. Even considering just simple Newtonian liquids, the systems of this type that can be treated exactly in the Oseen limit have until now been limited to either (a) two particles [14] or (b) an infinite linear

array of particles [15]. Clearly only the first case is experimentally accessible. There have been two experimental studies going beyond the two-sphere situation: the modes of motion in linear arrays of ten spheres have been studied in [15]; Di Leonardo *et al.* considered an arrangement of eight spheres at the vertices of a regular octagon [16]. In both cases, the eigenmodes of system and their dynamics were calculated approximately and compared to the observed cross-correlated motions (with good agreement). In this paper we show that the dynamics of systems where spheres are positioned on the vertices of arbitrary planar regular polygons can be solved *exactly* within Oseen's description of hydrodynamics. We use this powerful theoretical result to analyze the dynamical modes of systems from three to ten spheres, regularly positioned on a ring to form polygonal structures, and compare these predictions to experimental results.

II. EXPERIMENTAL SYSTEM

Optical traps are used to confine colloidal beads within harmonic potentials; the system hardware is described in greater detail in [7]. In this work, a varying number of silica beads of radius $a=1.75 \mu\text{m}$ (Bangslabs) are trapped by a time-shared laser beam. A pair of acousto-optical deflectors (AODs) allows the positioning of the laser beam in the (x, y) plane with subnanometer precision and at a rate high enough that a bead does not diffuse significantly in the time that the beam cycles through the other beads.

The solvent in which the beads are suspended is a glycerol (Fisher, Analysis Grade) water (Ultrapure grade, ELGA) solution 50% w/w, giving a nominal viscosity of $\eta = 6.00 \text{ mPa s}$ at $20 \text{ }^\circ\text{C}$ [17]. Experiments are performed in a temperature controlled laboratory, $T=21 \text{ }^\circ\text{C}$. The trapping plane is positioned $20 \pm 1 \mu\text{m}$ above the flat bottom of the sample, in a sample volume that is around $100 \mu\text{m}$ thick.

A trapped colloidal particle undergoes overdamped stochastic motion, driven by thermal forces which include the indirect effect of fluctuations of all other particles [14]. If only one bead is present in the system, its motion in the

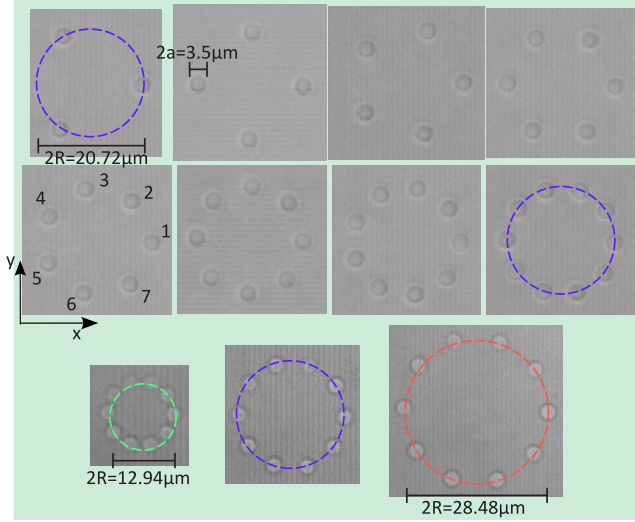


FIG. 1. (Color online) The experimental systems. Optical traps are created in a regular planar configuration, more than ten particle diameters away from solid boundaries. The traps act as springlike forces, confining each colloidal sphere to an average equilibrium position. Thermal noise causes displacements from the trap minima, and these fluctuations are correlated because of hydrodynamic interaction. Each panel shows one frame from the video obtained in the optical trap setup. Panels cover the range of configurations studied in this work: the top two rows show changes in N , whereas the change in R is illustrated in the bottom row. Changes in κ are also studied. Dashed lines are circles of the radii R studied experimentally, and values of R are indicated.

harmonic trap is characterized by the autocorrelation of each coordinate following $\langle x(t)x(t+\tau) \rangle = \langle x(t)^2 \rangle \exp(-\tau/\tau_0)$, with the relaxation time $\tau_0 = \gamma_0/\kappa$, where κ is the trap stiffness and the friction coefficient is $\gamma_0 = 6\pi\eta a$. The mean static amplitude is $\langle x(t)^2 \rangle = k_B T/\kappa$. A calibration experiment to obtain the trap stiffness consists of switching on the time-shared multi-point trap with only one particle present in the system (in one of the confining positions); by analyzing both $\langle x(t)^2 \rangle$ and τ_0 both the trapping stiffness of the trap and the sample viscosity in the experimental condition are obtained [18].

Experiments are performed increasing the number of beads N with beads confined to separate harmonic wells as shown in Fig. 1. The circle radius is labeled R and the distance between bead centers is $d = 2R \sin(\pi/N)$. In this set of experiments, the trap stiffness is maintained constant and $\tau_0 = 0.28$ s. N is varied from $N=3$ to 10 and the radius is fixed at $R = 10.36$ μm . To maintain the same trap stiffness across the experiments, the optical beam is always shared between ten trap locations, with only N traps positioned on the ring and occupied by beads. The laser beam is made to cycle through each trap position in a random order each cycle. The time spent by the beam at each trap position per cycle is around 50 μs . In another set of experiments, for $N=10$, the ring radius R is varied, and the trap strength κ is increased to give $\tau_0 = 0.16$ s and $\tau_0 = 0.11$ s. Overall the trap stiffness was varied in the range $0.7 \times 10^{-6} < \kappa < 2.0 \times 10^{-6}$ N/m.

Image acquisition is through an AVT Marlin F-131B complementary metal-oxide semiconductor camera, operat-

ing at shutter aperture time of 1.5 ms. The frame rate was 190 frames/s for the rings with largest R and 360 frames/s for the smallest R . Most data sets correspond to 15 min of video, i.e., over 250 000 frames. Multiple data sets are acquired for each parameter set.

III. THEORETICAL ANALYSIS

This section builds on the work of Polin *et al.*, where the hydrodynamic coupling of trapped beads is adequately described by a linearized Langevin-Oseen system [15]. Our theoretical contribution is the *exact* evaluation of eigenvalues and eigenvectors of the Oseen matrix (the Oseen matrix is a matrix representation of the Oseen tensor) for arbitrary regular polygonal arrangements of spheres. This provides an analytical description of the dynamics of the system with hydrodynamic interactions in the Oseen limit. The key steps of the derivation are given here, leading to a compact formula for the decay rates of the normal modes of the system. More details, useful for a reader to check and develop further, are presented in the Appendix.

The system of N colloidal spheres is localized in an array of harmonic wells at the vertices of a regular polygon of N sides. The beads are thermally excited, and they interact only through their influence on the surrounding medium. Indicating with $\mathbf{r}_j(t)$ the location of the j sphere at time t and \mathbf{R}_j the location of the center of its (stationary) trap, and by neglecting the inertial terms, the equations of motion for the spheres are described by the system

$$-\kappa[\mathbf{r}_i(t) - \mathbf{R}_i] - \sum_{j=1}^n \mathbf{H}_{ij}^{-1} \frac{d\mathbf{r}_j(t)}{dt} + \mathbf{f}_i(t) = 0, \quad (1)$$

where κ is the stiffness of each harmonic well, \mathbf{H}_{ij} is the Oseen matrix [10], and $\mathbf{f}_i(t)$ describes the thermal forces on the i particle. We assume the time averages $\langle \mathbf{f}_i(t) \rangle = 0$ and $\langle \mathbf{f}_i(t_1) \mathbf{f}_j(t_2) \rangle = 2k_B T \mathbf{H}_{ij}^{-1} \delta(t_1 - t_2)$. We focus from here onward on the plane (x, y) which contains the traps. Motion in z is decoupled and more difficult to observe experimentally in optical microscopy. Following again the previous analysis of [15], we replace the actual positions $\mathbf{r}_j(t)$ with the fixed ones \mathbf{R}_j inside the matrix \mathbf{H}_{ij} . As a result, the Oseen matrix is approximated by the real symmetric fixed matrix of order $2N$, so that

$$\gamma_0 H_{ij}^{\alpha\beta} = \delta_{ij} \delta_{\alpha\beta} + (1 - \delta_{ij}) \frac{3a}{4r_{ij}} \left(\delta_{\alpha\beta} + \frac{r_{ij}^{\alpha} r_{ij}^{\beta}}{r_{ij}^2} \right), \quad (2)$$

where $\alpha, \beta = 1, 2$ correspond to the x and y components, the indices $i, j = 1, \dots, N$ correspond to the sphere label, $\mathbf{r}_{ij} = \mathbf{R}_j - \mathbf{R}_i$, and $r_{ij} = |\mathbf{r}_{ij}|$. With the approximation of Eq. (2) the system of Eq. (1) has been turned into a system of coupled linear stochastic equations.

The collection of N two-dimensional positions $\{\mathbf{r}_j(t)\}$ can be arranged into a single $2N$ -dimensional vector $\{\mathbf{r}(t)\}$, and the same for the equilibrium positions $\{\mathbf{R}_j\} \rightarrow \{\mathbf{R}\}$. Let us call $\{\lambda_k\}, \{\mathbf{e}_k\}$ the collections of eigenvalues and orthonormal eigenvectors of the adimensional symmetric matrix $\gamma_0 \mathbf{H}_{ij}$, and O the orthogonal $2N$ -dimensional matrix built with them (the eigenvalues are the columns of O ; see the Appendix).

The system of equations (1) transforms into a system of decoupled equations for the normal modes $\xi(t) = O^{-1}(\mathbf{r}(t) - \mathbf{R})$,

$$-\kappa \xi_i(t) - \frac{\gamma_0}{\lambda_i} \frac{d}{dt} \xi_i(t) + \phi_i(t) = 0, \quad i = 1, 2, \dots, 2N, \quad (3)$$

where the thermal forces $\phi_i(t)$ have zero mean and with covariance [19]

$$\langle \phi_i(t_1) \phi_j(t_2) \rangle = 2k_B T \frac{\gamma_0}{\lambda_j} \delta_{ij} \delta(t_1 - t_2).$$

In the limit of strong damping the solutions of the system of Eq. (3) are expected to satisfy

$$\langle \xi_i(t) \xi_i(0) \rangle = C_i(0) e^{-t/\tau_i}, \quad (4)$$

where $C_i(0) = k_B T / \kappa$ and the relaxation times are $\tau_i = \gamma_0 / (\kappa \lambda_i)$.

By exploiting the symmetries of the polygonal array, it is possible to provide an analytical exact diagonalization of the matrix $\gamma_0 \mathbf{H}_{ij}$. This diagonalization is described in the Appendix and it may be of more general interest. The usefulness of the analytical approach may be appreciated from the results we anticipate here.

A. Analytical result for the decay times

Let $\omega = e^{-2\pi i/N}$ be a root of unity and $a_{j,N} = \sum_{k=1}^{N-1} \omega^{jk} \frac{1}{\sin(k\pi/N)}$. The $2N$ eigenvalues of the matrix $\gamma_0 \mathbf{H}_{ij}$ are

$$\begin{aligned} \lambda_{\mp} &= 1 + \frac{3a}{32R} [3(a_{j+1,N} + a_{j-1,N}) \\ &\quad \mp \sqrt{4a_{j,N}^2 + 9(a_{j+1,N} - a_{j-1,N})^2}], \\ &j = 1, 2, \dots, N. \end{aligned} \quad (5)$$

This formula is valid for any N and fully describes the dynamics of the system as R is varied. The effect of the trap stiffness κ is simply to set the overall time scale, with γ_0 .

B. Structure and distribution of modes with even N

For every even value of N (we studied experimentally $N = 4, 6, 8, 10$) the eigenmode corresponding to the longest relaxation time describes pairs of adjacent spheres moving tangentially to the ring in an antiphase synchronized motion. In Fig. 2 the eigenvalues of the matrix M (see the Appendix) are plotted on the horizontal axis (for $N = 8, 10, 12$) and their multiplicity is plotted on the vertical axis. The large majority of eigenvalues are negative, corresponding to relaxation times longer than they would be in the absence of hydrodynamic interaction. The most negative eigenvalue is the (non-degenerate) antiphase tangential motion. This is the slowest mode. The other two nondegenerate states are a coherent (in-phase) radial motion and a radial motion with nearest neighbors in antiphase; their order depends on N , as discussed in the Appendix.

There are always three modes (two of which degenerate) that have positive eigenvalues: here, the hydrodynamic interaction induces a decay faster than τ_0 . The nondegenerate

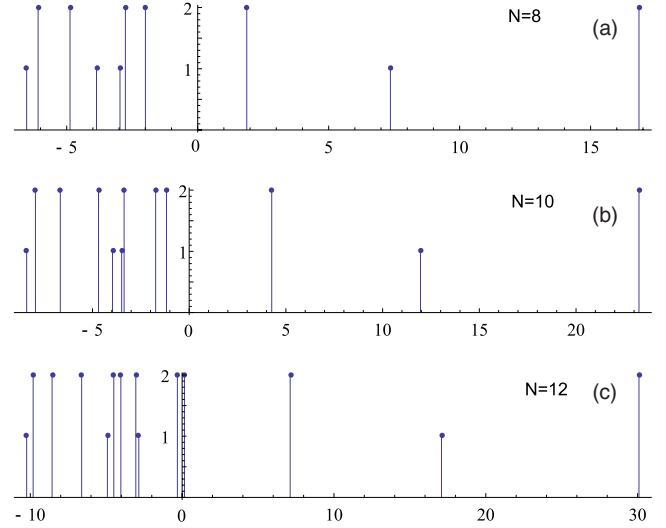


FIG. 2. (Color online) Distribution of eigenvalues reveals a general structure of mode dynamics. The degeneracy (one or two) of each mode is plotted as a function of the eigenvalue m of the matrix M defined in Eq. (A1). Negative eigenvalues correspond to relaxation times that are longer than τ_0 , and vice versa positive eigenvalues correspond to modes that are accelerated by the hydrodynamic interaction. The eigenvalues of the matrix $\gamma_0 \mathbf{H}$ are given by $\lambda = 1 + \frac{3a}{8R} m$. λ 's are inversely proportional to the time scales of mode relaxation and are all positive, meaning that the modes of the physical system are all overdamped.

mode is the coherent tangential motion. The fastest of all $2N$ modes is always degenerate, and it is a collective displacement of the entire ring in the plane (note that the structure of this mode is not trivial: the displacements of each bead are not exactly equal nor parallel).

IV. DATA ANALYSIS

A. Tracking

The bright-field images obtained from video data are analyzed using custom software coded in C, in which the first step of image correlation with an optimized kernel is followed by a two-dimensional fit near the maximum of the filtered image. This technique is well known to provide subpixel resolution, and in our experimental conditions the image analysis resolution is around 5 nm. This step results in an array of the (x, y) coordinates for each particle in the ring, as a function of time. Image analysis is not a relevant source of error in these experiments. Instead, like in previous work [15], we found that long time drift of the trap positions (on the order of a few tens of nm over 10 min) could not be avoided. Therefore, long time drift is removed from the data by removing the mean value over a moving window of 1000 frames; this cuts off low frequencies, corresponding to displacement time scales much longer than the longest expected relaxation time.

B. From coordinates to normal modes

The fluctuations of individual beads from their mean position form a set of $2N$ time series, with the displacements

along the axes: $\delta x(t)_i$ and $\delta y(t)_i$. In order to link with the analytical theory as outlined in this work, the displacements are measured in the (x, y) plane, with the axes as drawn in Fig. 1. The bead index increases anticlockwise and the bead with index=1 has a tangent to the trap ring parallel to y . Relative to this ideal condition, the experiments (due to AOD and camera mounts) have a small angular displacement, which is measured using the entire data set and then removed by a rotation of the $(\delta x, \delta y)$ displacement pairs.

At each time frame, the amplitudes of the $2N$ normal modes are obtained from the N displacement pairs $(\delta x(t)_i, \delta y(t)_i)$, through the matrix product $\xi(t) = O^{-1} * \{\delta x(t)_1, \delta y(t)_1, \delta x(t)_2, \delta y(t)_2, \dots, \delta x(t)_N, \delta y(t)_N\}$. The orthogonal matrix O is calculated analytically for each N , as described in the Appendix.

The autocorrelation in time of the normal-mode amplitudes is calculated and analyzed to obtain the experimental relaxation rates. The experimental autocorrelation function for each normal mode is expected to exhibit a simple exponential decay, and it can be compared to the theoretical expectation of Eq. (4) for the corresponding mode. The theoretically expected values of relaxation times are calculated analytically (see the Appendix) and are given by the very compact form of Eq. (5).

V. EXPERIMENTAL RESULTS AND DISCUSSION

If the motion of an individual particle within the system is considered, it is observed to have a complex dynamics. Its autocorrelation function in the radial and tangential components of the displacements would show multiple relaxation times, as a result of the hydrodynamic correlations between all particles in the ring. In contrast a single isolated particle shows simple exponential decay.

The autocorrelation functions $C(t)$ of the normal modes are shown in Fig. 3, for some of the experiments performed in this work. Each mode presents a simple exponential decay. The mode amplitude at $t=0$ is nearly constant for each mode, as expected theoretically. Fitting these relaxations with a simple exponential gives the relaxation time τ_j for the j mode. These times are compared to the exact theoretical prediction of Eq. (5), as shown in Fig. 4. There is excellent agreement between the theory and the experiments. By varying both R and N this data set extends the range of experimental time scales compared to previous work [15,16]. More importantly, the use of an exact theoretical formula allows us to focus on the origin of any remaining discrepancy between the observed behavior and the expected one. The most obvious discrepancy is the splitting of the fastest decaying mode. This mode is predicted to be twofold degenerate for any polygon; therefore, experimentally there should be two eigenmodes with the same short relaxation time scale. What is found instead is that the time scales split, and one of the modes is systematically slower than expected. The most likely explanation for this lies in a slight anisotropy of the individual optical traps, i.e., the rotational symmetry of each trap in the (x, y) plane is broken, resulting in breaking the degeneracy of modes that depended on this symmetry. Trap directional anisotropy is a well-known issue in laser trapping

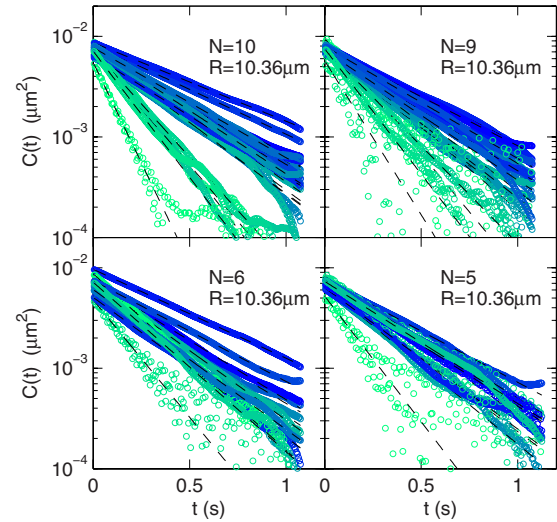


FIG. 3. (Color online) Autocorrelation functions of normal modes show simple exponential decay as a function of time. Data shown in the four panels are at fixed R and varying N . The number of normal modes is $2N$. Coding of shading for the data markers is from dark to light as the decay goes from slow to fast. Dashed lines are exponential fits; the corresponding relaxation times from this data (and many other experimental sets at different N , R , and κ) are plotted in Fig. 4.

due to imperfections in the optical setup. It is worth noting that even in a perfectly aligned setup the linear polarization of the laser beam would still result in a stiffness anisotropy of around 10% [20]. The directional anisotropy plays the strongest role on the fastest decaying mode because of its collective nature. In modes with higher symmetry the directional anisotropy is effectively averaged out.

The description of hydrodynamic interaction through Oseen's tensor and the linearization of the interaction matrix assuming a constant d are expected to hold for large bead separations (gaps that are large relative to the bead size and bead displacements, respectively). The gap size in this work ranges from $18 \mu\text{m}$ down to $0.57 \mu\text{m}$. The typical amplitude of displacements (root-mean-square thermal fluctuations) is $8 \times 10^{-2} \mu\text{m}$. Therefore, fluctuations are small relative to all the gap sizes explored here and might become important only for very weak trapping or (less practically) in the limit of high T . The data sets with smallest gap sizes might be expected to lie out of the Oseen description, but we do not observe deviations.

VI. CONCLUSIONS

The dynamics of planar polygonal structures of colloidal particles in a Newtonian liquid have been studied experimentally and theoretically, highlighting the role of hydrodynamic interaction. Developing previous work by other groups [14–16], the range of systems that are studied experimentally has been expanded. A theoretical treatment of the interaction matrix has yielded exact analytical results for the structure of dynamical modes and a particularly simple expression for the relaxation time scales of all modes. Aside from the fun-

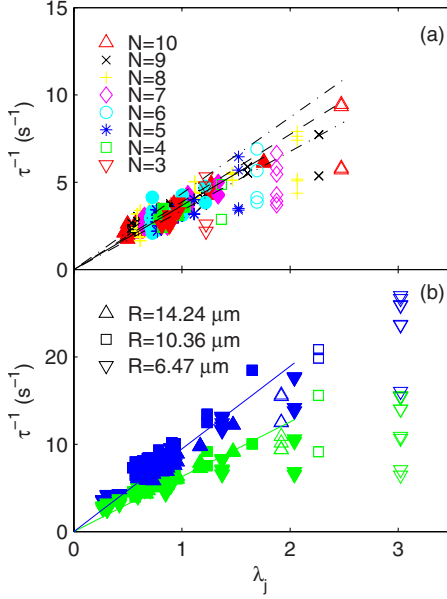


FIG. 4. (Color online) Comparison of experimental and theoretical results. The experimentally determined time scales for the relaxation of the $2N$ normal modes are in good agreement with the theoretical analysis. (a) shows experiments where N is varied. The dotted line is the analytical prediction from Eq. (5), using the value of γ_0 obtained from calibration. The dashed-dotted lines represent the boundaries corresponding to the standard deviation of γ_0 between calibration runs. In both panels, the fastest mode data are plotted in open symbols. For reasons that have something to do with the experimental setup and discussed in the text, the degeneracy of this mode is systematically broken. In (b) the number of beads is fixed to $N=10$. R is varied as noted in the legend, and for every R two values of κ are explored. The solid lines are best fits to a linear line through the origin showing good collapse of the data. The gradient of these lines is $\kappa/\gamma_0 = \tau_0^{-1}$, giving $\tau_0 = 0.16$ s and $\tau_0 = 0.11$ s for the weaker and stronger optical traps (lower and upper sets of data, respectively).

damental interest in the dynamical structure of this family of systems, we expect this work to underpin developments in two directions. First it would be natural to extend the multi-bead structures as probes for complex fluids, where in principle multiscale multiple-frequency data could be obtained simultaneously. The theoretical analysis becomes of course more complex and would require a generalization of the theory for two spheres in a viscoelastic medium [21]. The other area of development is to study the potential of these polygonal structures to form self-organized dynamical states, under local driving from the optical traps. This would extend our recent work on dynamical synchronization in pairs of colloidal particles [3]. Under these conditions it is possible that large displacements would occur, and the analytical results here would form the reference for a higher-order approximation.

The analytical diagonalization of the Oseen matrix is possible because of the symmetry of the regular polygon and the direct two-body forces, and it does not rely on the specific way of how they depend on the distance. Then it seems likely that an analogous diagonalization would be possible both for simpler cases (like particles on the ring, but includ-

ing the hydrodynamic interaction only for pairs of nearest neighbors) and for more complex ones (like replacing the Oseen tensor with the Rotne-Prager expression [22], for example). Such investigations may further elucidate the relevant effective hydrodynamic interaction for polygonal configurations of spheres.

ACKNOWLEDGMENTS

G.M.C. wishes to thank R. Di Leonardo for communicating details regarding Ref. [15]. We also acknowledge useful discussions with M. Cosentino Lagomarsino and B. Bassetti.

APPENDIX: ANALYTICAL CALCULATION OF NORMAL MODES

The Oseen matrix in Eq. (2) of order $2N$ may be conveniently regarded as a matrix of order N where each entry (i, j) is a matrix of order 2. Our method is to transform, by a similarity, the matrix into a circulant matrix of order N where the entry (i, j) is a matrix of order 2. Eigenvalues and eigenvectors of the latter matrix are easily found by the same methods used for ordinary circulant matrices [23,24].

Let us choose the origin of Cartesian coordinates at the center of the ring of radius R and label the equilibrium position of the particles counterclockwise. The center of the j particle has coordinates

$$\begin{pmatrix} \mathbf{r}_{jx} \\ \mathbf{r}_{jy} \end{pmatrix} = R \begin{pmatrix} \cos 2\pi(j-1)/N \\ \sin 2\pi(j-1)/N \end{pmatrix}, \quad j = 1, 2, \dots, N,$$

and the coordinates of the differences of vectors are

$$\vec{r}_{ij} = \mathbf{r}_j - \mathbf{r}_i = 2R \begin{pmatrix} -\sin \frac{(j+i-2)\pi}{N} \sin \frac{(j-i)\pi}{N} \\ \cos \frac{(j+i-2)\pi}{N} \sin \frac{(j-i)\pi}{N} \end{pmatrix}.$$

The distance r_{ij} between the positions i, j is $r_{ij} = 2R \sin \frac{|j-i|\pi}{N}$. The largest number of solid spheres which may be placed on the ring is N_{\max} , being the largest integer such that $\sin(\pi/N_{\max}) > a/R$.

We then rewrite the Oseen matrix in Eq. (2), so that

$$\begin{aligned} \gamma_0 H_{ij}^{\alpha\beta} &= \delta_{ij} \delta_{\alpha\beta} + (1 - \delta_{ij}) \frac{3a}{8R \sin \frac{|j-i|\pi}{N}} \left(\delta_{\alpha\beta} + \frac{r_{ij}^\alpha r_{ij}^\beta}{r_{ij}^2} \right) \\ &= \delta_{ij} \delta_{\alpha\beta} + \frac{3a}{8R} M_{ij}^{\alpha\beta}, \\ M_{ij}^{\alpha\beta} &= (1 - \delta_{ij}) \frac{1}{\sin \frac{|j-i|\pi}{N}} \left(\delta_{\alpha\beta} + \frac{r_{ij}^\alpha r_{ij}^\beta}{r_{ij}^2} \right). \end{aligned} \quad (\text{A1})$$

The Oseen matrix $\gamma_0 H_{ij}^{\alpha\beta}$ and the matrix M share the same eigenvectors, and for a given eigenvalue m of the matrix M the matrix $\gamma_0 H_{ij}^{\alpha\beta}$ has the eigenvalue $\lambda = 1 + \frac{3a}{8R} m$.

Let us define the orthogonal matrix u and the diagonal matrix b , both of order 2,

$$u = \begin{pmatrix} \cos \frac{\pi}{N} & \sin \frac{\pi}{N} \\ -\sin \frac{\pi}{N} & \cos \frac{\pi}{N} \end{pmatrix},$$

$$u^k = \begin{pmatrix} \cos \frac{k\pi}{N} & \sin \frac{k\pi}{N} \\ -\sin \frac{k\pi}{N} & \cos \frac{k\pi}{N} \end{pmatrix},$$

$$b = \begin{pmatrix} 1 & 0 \\ 0 & 2 \end{pmatrix},$$

then

$$M_{ij}^{\alpha\beta} = (1 - \delta_{ij}) \frac{1}{\sin \frac{|j-i|\pi}{N}} (u^{2-i-j} \cdot b \cdot u^{i+j-2})^{\alpha\beta}.$$

Let us define the two block-diagonal matrices

$$S = \begin{pmatrix} u^0 & & & & & \\ & u^2 & & & & \\ & & u^4 & & & \\ \dots & \dots & \dots & \dots & \dots & \\ & & & & & u^{2N-2} \end{pmatrix},$$

$$S^{-1} = \begin{pmatrix} u^0 & & & & & \\ & u^{-2} & & & & \\ & & u^{-4} & & & \\ \dots & \dots & \dots & \dots & \dots & \\ & & & & & u^{-2N} \end{pmatrix}.$$

The matrix $\tilde{M} = S \cdot M \cdot S^{-1}$ is block circulant,

$$\tilde{M} = \begin{pmatrix} 0 & \frac{u^{-1} \cdot b \cdot u^{-1}}{\sin \pi/N} & \frac{u^{-2} \cdot b \cdot u^{-2}}{\sin 2\pi/N} & \frac{u^{-3} \cdot b \cdot u^{-3}}{\sin 3\pi/N} & \dots & \dots & \frac{u^{-(N-1)} \cdot b \cdot u^{-(N-1)}}{\sin(N-1)\pi/N} \\ \frac{u^1 \cdot b \cdot u^1}{\sin \pi/N} & 0 & \frac{u^{-1} \cdot b \cdot u^{-1}}{\sin \pi/N} & \frac{u^{-2} \cdot b \cdot u^{-2}}{\sin 2\pi/N} & \dots & \dots & \frac{u^{-(N-2)} \cdot b \cdot u^{-(N-2)}}{\sin(N-2)\pi/N} \\ \frac{u^2 \cdot b \cdot u^2}{\sin 2\pi/N} & \frac{u^1 \cdot b \cdot u^1}{\sin \pi/N} & 0 & \frac{u^{-1} \cdot b \cdot u^{-1}}{\sin \pi/N} & \dots & \dots & \frac{u^{-(N-3)} \cdot b \cdot u^{-(N-3)}}{\sin(N-3)\pi/N} \\ \frac{u^3 \cdot b \cdot u^3}{\sin 3\pi/N} & \frac{u^2 \cdot b \cdot u^2}{\sin 2\pi/N} & \frac{u^1 \cdot b \cdot u^1}{\sin \pi/N} & 0 & \dots & \dots & \frac{u^{-(N-4)} \cdot b \cdot u^{-(N-4)}}{\sin(N-4)\pi/N} \\ \dots & \dots & \dots & \dots & \dots & \dots & \dots \\ \frac{u^{(N-2)} \cdot b \cdot u^{(N-2)}}{\sin(N-2)\pi/N} & \frac{u^{(N-3)} \cdot b \cdot u^{(N-3)}}{\sin(N-3)\pi/N} & \frac{u^{(N-4)} \cdot b \cdot u^{(N-4)}}{\sin(N-4)\pi/N} & \dots & \dots & 0 & \frac{u^{-1} \cdot b \cdot u^{-1}}{\sin \pi/N} \\ \frac{u^{(N-1)} \cdot b \cdot u^{(N-1)}}{\sin(N-1)\pi/N} & \frac{u^{(N-2)} \cdot b \cdot u^{(N-2)}}{\sin(N-2)\pi/N} & \frac{u^{(N-3)} \cdot b \cdot u^{(N-3)}}{\sin(N-3)\pi/N} & \frac{u^{(N-4)} \cdot b \cdot u^{(N-4)}}{\sin(N-4)\pi/N} & \dots & \dots & 0 \end{pmatrix}.$$

Let $\omega = e^{-2\pi i/N}$. For any fixed j ($1 \leq j \leq N$), one obtains two eigenvalues, say $m_{j,\pm}$, of the matrix \tilde{M} by solving the quadratic equation resulting from the entries of the first row of the matrix,

$$\det \left[-m\mathbb{I} + \omega^j \frac{u^{-1} \cdot b \cdot u^{-1}}{\sin \pi/N} + \omega^{2j} \frac{u^{-2} \cdot b \cdot u^{-2}}{\sin 2\pi/N} + \dots + \omega^{j(N-1)} \frac{u^{-(N-1)} \cdot b \cdot u^{-(N-1)}}{\sin(N-1)\pi/N} \right] = 0.$$

Let $[m^{(j,\pm)}]$ be the two eigenvectors of the matrix

$A_j = \sum_{k=1}^{N-1} \omega^{jk} [u^{-k} \cdot b \cdot u^{-k} / (\sin k\pi/N)]$ of order 2, then the corresponding two eigenvectors of the matrix \tilde{M} may be written as a direct product of an N -component vector $[\Omega_j]$ times the two-component eigenvectors $[m^{(j,\pm)}]$,

$$[\Omega_j][m^{(j,+)}] = \begin{bmatrix} [m^{(j,+)}] \\ \omega^j [m^{(j,+)}] \\ \omega^{2j} [m^{(j,+)}] \\ \dots \\ \omega^{j(N-1)} [m^{(j,+)}] \end{bmatrix},$$

TABLE I. The relaxation times of polygonal structures can be calculated analytically, and a particularly compact form exists for the case of even N . The minimum and maximum eigenvalues for the first six even N structures are evaluated here using Eq. (A2).

	$N=4$	$N=6$	$N=8$	$N=10$	$N=12$	$N=14$
m_{\min}	-2.414	-4.577	-6.528	-8.402	-10.239	-12.054
m_{\max}	5.772	10.964	16.846	23.254	30.089	37.285

$$[\Omega_j] \times [m^{(j,-)}] = \begin{bmatrix} [m^{(j,-)}] \\ \omega^j [m^{(j,-)}] \\ \omega^{2j} [m^{(j,-)}] \\ \dots \\ \omega^{j(N-1)} [m^{(j,-)}] \end{bmatrix},$$

with

$$[\Omega_j] = \begin{bmatrix} 1 \\ \omega^j \\ \omega^{2j} \\ \dots \\ \omega^{j(N-1)} \end{bmatrix}.$$

Finally, the corresponding eigenvector for the matrix M (and therefore also for the Oseen matrix) is $S^{-1}([\Omega_j] \times [m^{(j,\pm)}])$.

The eigenvectors of the matrix M can be arranged as columns to form a unitary complex matrix. By taking linear combinations of the pairs of complex eigenvectors that correspond to the double-degenerate eigenvalues, one may have real eigenvectors and a real orthogonal matrix which we name O . Either the unitary matrix or the orthogonal one may be used to analyze the experimentally measured covariance matrix of the displacements of the particles from the equilibrium positions.

The similarity of the previous analysis with the more usual discrete Fourier transform, valid for periodic systems on a line [25], is apparent. The only different complications occurring here are the similarity transform, related to periodicity on the ring, and the two-dimensional entries.

Evaluations and comments

The evaluations are greatly simplified by simple observations. Since we know the eigenvectors of u^k ,

$$u^k \begin{bmatrix} 1 \\ i \end{bmatrix} = e^{k\pi i/N} \begin{bmatrix} 1 \\ i \end{bmatrix}, \quad u^k \begin{bmatrix} i \\ 1 \end{bmatrix} = e^{-k\pi i/N} \begin{bmatrix} i \\ 1 \end{bmatrix},$$

one finds the action of A_j on these two vectors,

$$u^k \cdot b \cdot u^k \begin{bmatrix} 1 \\ i \end{bmatrix} = \frac{3}{2} e^{2k\pi i/N} \begin{bmatrix} 1 \\ i \end{bmatrix} + \frac{i}{2} \begin{bmatrix} i \\ 1 \end{bmatrix},$$

$$u^k \cdot b \cdot u^k \begin{bmatrix} i \\ 1 \end{bmatrix} = -\frac{i}{2} \begin{bmatrix} 1 \\ i \end{bmatrix} + \frac{3}{2} e^{-2k\pi i/N} \begin{bmatrix} i \\ 1 \end{bmatrix},$$

$$A_j \begin{bmatrix} 1 \\ i \end{bmatrix} = \frac{3}{2} a_{j+1,N} \begin{bmatrix} 1 \\ i \end{bmatrix} + \frac{i}{2} a_{j,N} \begin{bmatrix} i \\ 1 \end{bmatrix},$$

$$A_j \begin{bmatrix} i \\ 1 \end{bmatrix} = -\frac{i}{2} a_{j,N} \begin{bmatrix} 1 \\ i \end{bmatrix} + \frac{3}{2} a_{j-1,N} \begin{bmatrix} i \\ 1 \end{bmatrix},$$

where

$$a_{j,N} = \sum_{k=1}^N \omega^{jk} \frac{1}{\sin k\pi/N}.$$

Since these vectors are a basis in the two-dimensional space, one finds all the eigenvalues of the Oseen matrix by evaluating the eigenvalues of A_j ,

$$m_{j,\pm} = \frac{1}{4} [3(a_{j+1,N} + a_{j-1,N}) \pm \sqrt{4a_{j,N}^2 + 9(a_{j+1,N} - a_{j-1,N})^2}]. \quad (\text{A2})$$

For various values of N the pattern of eigenvalues has common features of some significance. For every N even integer, the matrix M (and equivalently the Oseen matrix) has $N-2$ double-degenerate eigenvalues and four singlet eigenvalues, originating from the matrices $A_{N/2}$ and A_N . The minimum eigenvalue is physically the most important, as it corresponds to the eigenmode with the longest relaxation time. For every even N ($4 \leq N$), it is the singlet eigenvalue $m_{N/2,-}$,

$$m_{\min} = m_{N/2,-} = \frac{1}{2} (3a_{N/2+1,N} - |a_{N/2,N}|).$$

The corresponding eigenmode describes particles moving along the tangent of the ring, with adjacent particles moving in opposite versus. The fact that the antiphase mode has the longest relaxation time is related to the observed synchronized state of a pair of driven oscillators with hydrodynamic coupling, which also exhibits near-antiphase structure [3]. Antiphase is a general property of the steady state of driven oscillators with viscous coupling [26].

Also the other three singlet eigenvalues are associated with eigenmodes that are easily described. The second eigenvalue from the matrix $A_{N/2}$ is $m_{N/2,+} = \frac{1}{2} (3a_{N/2+1,N} + |a_{N/2,N}|)$. Its eigenmode describes beads moving radially, where adjacent beads have opposite versus. The remaining two singlet eigenvalues originate from the matrix A_N . The corresponding eigenmodes describe beads moving tangent to the ring, with coherent versus (the eigenvalue $m_{N,-}$) or beads moving radially to the ring, with coherent versus (the eigenvalue $m_{N,+}$). The order of $m_{N/2,+}$ and $m_{N,-}$ varies with N . The largest eigenvalue (fastest relaxation) is always doubly degenerate; it is $m_{1,+} = m_{N-1,+}$.

The range of values for the maximum and minimum eigenvalues of the first six even rings is shown in Table I. For N odd integer, the matrix M , hence also the Oseen matrix, has $N-1$ double-degenerate eigenvalues and two singlet ei-

genvalues, originating from the matrix A_N . The minimum eigenvalue is a singlet for $N=3$ and 5, but it is doubly degenerate for $N \geq 7$, then corresponding to $m_{(N+1)/2,-} = m_{(N-1)/2,-}$.

-
- [1] M. Polin, I. Tuval, K. Drescher, J. Gollub, and R. Goldstein, *Science* **325**, 487 (2009).
- [2] S. Gueron, K. Levit-Gurevich, N. Liron, and J. Blum, *Proc. Natl. Acad. Sci. U.S.A.* **94**, 6001 (1997).
- [3] J. Kotar, M. Leoni, B. Bassetti, M. Cosentino Lagomarsino, and P. Cicuta, *Proc. Natl. Acad. Sci. U.S.A.* **107**, 7669 (2010).
- [4] T. Beatus, T. Tlustý, and R. Bar-Ziv, *Nat. Phys.* **2**, 743 (2006).
- [5] P. Hänggi and F. Marchesoni, *Rev. Mod. Phys.* **81**, 387 (2009).
- [6] V. B. Putz and J. M. Yeomans, *J. Stat. Phys.* **137**, 1001 (2009).
- [7] M. Leoni, J. Kotar, B. Bassetti, P. Cicuta, and M. Cosentino Lagomarsino, *Soft Matter* **5**, 472 (2009).
- [8] E. Lauga and T. R. Powers, *Rep. Prog. Phys.* **72**, 096601 (2009).
- [9] M. Leoni, B. Bassetti, J. Kotar, P. Cicuta, and M. Cosentino Lagomarsino, *Phys. Rev. E* **81**, 036304 (2010).
- [10] J. Happel and H. Brenner, *Low Reynolds Number Hydrodynamics: With Special Applications to Particulate Media* (Kluwer, New York, 1983).
- [11] T. A. Waigh, *Rep. Prog. Phys.* **68**, 685 (2005).
- [12] P. Cicuta and A. M. Donald, *Soft Matter* **3**, 1449 (2007).
- [13] A. M. Yao, S. A. J. Keen, D. R. Burnham, R. Leach, R. Di Leonardo, D. McGloin, and M. J. Padgett, *New J. Phys.* **11**, 053007 (2009).
- [14] J. C. Meiners and S. R. Quake, *Phys. Rev. Lett.* **82**, 2211 (1999).
- [15] M. Polin, D. G. Grier, and S. Quake, *Phys. Rev. Lett.* **96**, 088101 (2006).
- [16] R. Di Leonardo, S. Keen, J. Leach, C. D. Saunter, G. D. Love, G. Ruocco, and M. J. Padgett, *Phys. Rev. E* **76**, 061402 (2007).
- [17] R. C. Weast and M. J. Astle, *CRC Handbook of Chemistry and Physics*, 60th ed. (CRC Press, Boca Raton, FL, 1979).
- [18] As usual in experiments on optically trapped colloids, due to uncertainty in the exact bead size and local temperature, the measured calibration values of κ and γ_0 are considered as more meaningful than the stiffness κ that could be calculated from momentum transfer, or γ_0 obtained by assuming the nominal or bulk measured solvent viscosity.
- [19] Apparently a misprint occurs in Eq. (8) of Ref. [15].
- [20] T. Wohland, A. Rosin, and E. H. K. Stelzer, *Optik (Stuttgart)* **102**, 181 (1996).
- [21] D. T. Chen, E. R. Weeks, J. C. Crocker, M. F. Islam, R. Verma, J. Gruber, A. J. Levine, T. C. Lubensky, and A. G. Yodh, *Phys. Rev. Lett.* **90**, 108301 (2003).
- [22] J. Rotne and S. Prager, *J. Chem. Phys.* **50**, 4831 (1969).
- [23] M. Mehta, *Matrix Theory* (Les Editions de Physique, Les Ulis, 1989).
- [24] P. Davis, *Circulant Matrices* (Wiley, New York, 1979).
- [25] M. Mehta, *J. Math. Phys.* **28**, 781 (1987).
- [26] A. Pikovsky, M. Rosenblum, and J. Kurths, *Synchronization* (Cambridge University Press, Cambridge, UK, 2001).